INSTITUTE OF PHYSICS PUBLISHING JOURNAL OF PHYSICS B: ATOMIC, MOLECULAR AND OPTICAL PHYSICS

J. Phys. B: At. Mol. Opt. Phys. **35** (2002) 783–793 PII: S0953-4075(02)26532-3

Elastic scattering of low-energy electrons by NF_3

E Joucoski and M H F Bettega

Departamento de Física, Universidade Federal do Paraná, Caixa Postal 19044, 81531-990, Curitiba, Paraná, Brazil

Received 29 June 2001, in final form 29 November 2001
Published 13 February 2002
Online at stacks.iop.org/JPhysB/35/783

Abstract

We present results of e^-–NF_3 collision calculations for energies up to 60 eV. To compute the elastic integral, differential, and momentum-transfer cross sections we have employed the Schwinger multichannel method implemented with norm-conserving pseudopotentials (Bettega M H F, Ferreira L G and Lima M A 1993 *Phys. Rev.* A **47** 1111) within the fixed-nuclei static-exchange approximation. We have compared our results with the complex Kohn results of Rescigno and with the experimental data of Boesten *et al*, and found them in general good agreement. We have found two independent shape resonances in the NF_3 elastic integral cross section, and through its symmetry decomposition we assigned them to the A_1 and E representations of the C_{3v} group. The existence of a shape resonance has also been reported by Rescigno and also by Boesten *et al*, who assigned it to the E representation of the C_{3v} group. We have also discussed the possible role of these shape resonances in the dissociative attachment of NF_3 by electron impact.

1. Introduction

An explanation of the importance of NF_3 in processes of plasma etching can be found in several works available in the literature [1]. NF_3 has been used as an etchant gas as an alternative to the common perfluorocarbon (PCF) gases for two reasons, namely, there is no formation of polymer residues during the etching and it is more environmentally compatible than the PCFs [2]. It has also been used in plasma discharge experiments in cleaning elements such as UO_2 from metallic substrates [3].

Modelling plasma discharges requires previous knowledge in several different areas. For example, thermochemistry data on the neutrals and ions as well as the elastic, inelastic, and ionization cross sections resulting from the collisions of the electrons with the neutral molecules of the gas represent very important information for plasma modellers. Also, they help in the understanding of the basic processes that occur in the plasma. This subject has been discussed in a recent paper by Winstead and McKoy [4].

Despite the importance of the NF_3 molecule in technological applications, little is known about e^-–NF_3 collision processes. As regards low-energy electron scattering by NF_3, we can

0953-4075/02/040783+11$30.00

cite the complex Kohn elastic and inelastic e^-–NF_3 collision calculations by Rescigno [5], and the experiments by Boesten *et al* [6] on vibrationally inelastic and elastic e^-–NF_3 collisions. Both works have reported the formation of a shape resonance during the collision. We can also quote calculations of the electron-impact ionization cross section of NF_3 [7], experiments on dissociative attachment of NF_3 by electron impact [8, 9], and calculations of the adiabatic ionization potential and enthalpies of formation [10].

As the outcome of the dissociative attachment experiments, there were found F^- ions, reported to be the most dominant channel, and also F_2^- and NF_2^- ions [8, 9]. In electron–molecule collisions, electron attachment appears as shape resonances or temporary anion states formed during the collision. As cited above, Rescigno and Boesten *et al* reported the existence of a shape resonance in the elastic cross section of NF_3. Rescigno found a shape resonance in the elastic momentum-transfer cross section (MTCS) at 5.5 eV. However, he has not discussed to which symmetry the resonance belongs. On the basis of this result, Rescigno was inclined to believe that this shape resonance was responsible for the dissociative attachment of NF_3. Boesten *et al* found in the vibrational excitation function a shape resonance at 3 eV and assigned it to the E representation of the C_{3v} group. As a complementary study to the previous works available in the literature, we present in this work results of our calculations on elastic scattering of low-energy electrons by NF_3 molecules. To compute the elastic integral, differential and momentum-transfer cross sections, we have used the Schwinger multichannel (SMC) method with pseudopotentials (SMCPP) [11]. Our calculations were performed under the fixed-nuclei static-exchange (SE) approximation. Our aim is to provide reliable elastic cross sections for energies where the SE works well and also to explore the shape resonance found in the elastic channel.

In the following sections we present the theoretical formulation of our method, the computational procedures used in our calculations, and our results and discussion. We end this paper with a brief summary of our findings.

2. Theory

The SMC method [12, 13] has been described in detail in several publications, and we will review here only the steps which are important to this work. The SMC method uses a variational approximation to the scattering amplitude, where the scattering wavefunction is expanded in a basis set consisting of $(N + 1)$-electron Slater determinants $\{|\chi_m\rangle\}$ as follows:

$$|\Psi_{\vec{k}}^{(\pm)}\rangle = \sum_m a_m^{(\pm)}(\vec{k})|\chi_m\rangle. \tag{1}$$

The coefficients $\{a_m^{(\pm)}(\vec{k})\}$ of the above expansion are determined through a variational approach. The resulting expression for the scattering amplitude is

$$[f_{\vec{k}_i,\vec{k}_f}] = -\frac{1}{2\pi}\sum_m\sum_n \langle S_{\vec{k}_f}|V|\chi_m\rangle (d^{-1})_{mn}\langle\chi_n|V|S_{\vec{k}_i}\rangle, \tag{2}$$

where

$$d_{mn} = \langle\chi_m|A^{(+)}|\chi_n\rangle, \tag{3}$$

and

$$A^{(+)} = \frac{\hat{H}}{N+1} - \frac{(\hat{H}P + P\hat{H})}{2} + \frac{(VP + PV)}{2} - VG_P^{(+)}V. \tag{4}$$

In the above equations, $|S_{\vec{k}_i}\rangle$ is the solution for the unperturbed Hamiltonian H_0 and is given by the product of a target state and a plane wave, V is the interaction potential between the

incident electron and the target, $\{|\chi_m\rangle\}$ is a set of $(N+1)$-electron Slater determinants used in the expansion of the trial scattering wavefunction according to equation (1), $\hat{H} = E - H$ is the total energy of the collision minus the full Hamiltonian of the system, with $H = H_0 + V$. P is a projection operator projecting onto the open-channel space defined in terms of target eigenfunctions $|\Phi_l\rangle$:

$$P = \sum_{l=1}^{\text{open}} |\Phi_l\rangle\langle\Phi_l|, \tag{5}$$

and $G_P^{(+)}$ is the free-particle Green function projected on the P-space.

In a SE approximation calculation, where target polarization is completely neglected, the configuration space $\{|\chi_m\rangle\}$ is constructed as

$$|\chi_m\rangle = \mathcal{A}\{|\Phi_1\rangle|\varphi_m\rangle\}, \tag{6}$$

where $|\Phi_1\rangle$ is the target ground-state wavefunction, described at the Hartree–Fock level of approximation, $|\varphi_m\rangle$ is a one-electron function, and $\mathcal{A}$ is the antisymmetrizer. In this approximation, the projection operator is given by

$$P = |\Phi_1\rangle\langle\Phi_1|. \tag{7}$$

The numerical calculation of VGV demands the calculation of primitive two-electron integrals of the type

$$\langle\alpha\beta|V|\gamma\vec{k}\rangle = \int\int \mathrm{d}\vec{r}_1\,\mathrm{d}\vec{r}_2\,\alpha(\vec{r}_1)\beta(\vec{r}_1)\frac{1}{r_{12}}\gamma(\vec{r}_2)\mathrm{e}^{\mathrm{i}\vec{k}\cdot\vec{r}_2}, \tag{8}$$

which involve a plane wave and three Cartesian Gaussians and must be evaluated for all possible combinations of α, β and γ and for several directions and moduli of the wavevector $\vec{k}$. In a pseudopotential calculation the number of these two-electron integrals is reduced in comparison with an all-electron calculation. The price that we must pay in using pseudopotentials is to evaluate the one-electron integrals of the type

$$\langle\alpha|V^{PP}|\vec{k}\rangle = \int \mathrm{d}\vec{r}\,\alpha(\vec{r})V^{PP}\mathrm{e}^{\mathrm{i}\vec{k}\cdot\vec{r}}, \tag{9}$$

which are more complex than those from bound-state calculations involving the nuclei. However, they can be calculated analytically and their number is also reduced due to the use of smaller basis sets in pseudopotential calculations. In the above equation, V^{PP} is the nonlocal pseudopotential operator given by

$$\hat{V}^{PP}(r) = \hat{V}_{\text{core}}(r) + \hat{V}_{\text{ion}}(r), \tag{10}$$

with

$$\hat{V}_{\text{core}}(r) = -\frac{Z_{\text{v}}}{r}\left[\sum_{i=1}^{2} c_i^{\text{core}}\,\text{erf}[(\alpha_i^{\text{core}})^{1/2}r]\right], \tag{11}$$

and

$$\hat{V}_{\text{ion}}(r) = \sum_{n=0}^{1}\sum_{j=1}^{3}\sum_{l=0}^{2} A_{njl}r^{2n}\mathrm{e}^{-\alpha_{jl}r^2}\sum_{m=-l}^{+l}|lm\rangle\langle lm|, \tag{12}$$

where Z_{v} is the valence charge of the atom and in this application it is equal to 5 for nitrogen and 7 for fluorine. The coefficients c_i^{core}, A_{njl}, and the decay constants α_i^{core} and α_{jl} are tabulated in [14].

Table 1. Cartesian Gaussian function exponents for nitrogen and fluorine atoms.

Type	N exponent	F exponent	Coefficient
s	17.569 870	12.545 580	1.0
s	3.423 613	6.272 790	1.0
s	0.884 301	1.576 479	1.0
s	0.259 045	0.499 283	1.0
s	0.053 066	0.150 680	1.0
s	0.022 991	0.077 101	1.0
p	7.050 692	9.852 550	1.0
p	1.910 543	2.330 403	1.0
p	0.579 261	0.462 593	1.0
p	0.165 395	0.154 197	1.0
p	0.037 192	0.051 399	1.0
d	0.403 039	0.790 820	1.0
d	0.091 192	0.181 887	1.0

3. Computational procedures

Our e^-–NF_3 collision calculations were performed under the fixed-nuclei SE approximation, with the molecule in its ground-state equilibrium geometry with $R(\mathrm{NF}) = 1.365$ Å and $\angle(\mathrm{FNF}) = 102.3^\circ$ [5,6]. The cross sections were obtained by means of the SMC method with pseudopotentials. The $^1A_1$ ground-state wavefunction, $|\Phi_1\rangle$, was described by a single Slater determinant. The basis set used to describe the target ground state and the scattering orbitals in equation (6) are listed in table 1, and were obtained according to the recipes given in [15]. This basis set gives a total of 132 molecular orbitals, from which 13 are used to describe the ground-state wavefunction for the valence electrons as follows: four for the A_1 representation, four for each component of the E representation (twofold degenerate), and one for the A_2 representation. The virtual orbitals are used to construct the configuration space according to equation (6). Since we have not included in our calculations the symmetric combination of d-type functions, namely $[(x^2+y^2+z^2)\exp(-\alpha r^2)]$, in order to eliminate linear dependence in the basis set, we have a total of 111 scattering orbitals, distributed by symmetry as follows: 31 for A_1, 36 for each component of E, and 8 for A_2. The calculated dipole moment is 0.263 D, with agrees well with the calculated value of 0.282 D from [5] and with the experimental value of 0.235 D [16]. Due to the small size of the dipole moment of NF_3, we have omitted in our calculations the correction for long-range scattering by the dipole potential [17,18].

4. Results

Figure 1 shows our calculated integral cross section (ICS) and the experimental results of Boesten *et al*. Our ICS lies above the experimental data for energies above 5 eV and shows a shape resonance around 7 eV. From the symmetry decomposition of the ICS according to the C_{3v} group, also shown in figure 1, we found that in fact there are two independent shape resonances belonging to the A_1 and E representations of this group.

In figures 2–5 we compare our calculated differential cross sections (DCSs) with the experimental DCS of Boesten *et al*. In figure 2 we present the DCSs at 4 and 5 eV, which are energies just below the peak, where we found good agreement between theory and experiment. In figure 3 we show the DCSs at 7, 8, and 10 eV. These energies correspond to the resonance region, and the agreement between theory and experiment becomes poorer. Figures 4 and 5

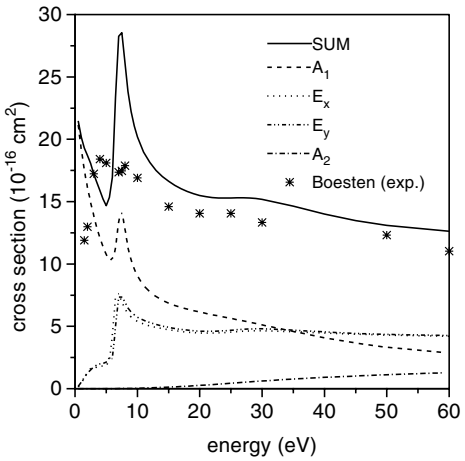

Figure 1. The ICS of NF_3.

Table 2. Integral, differential and momentum-transfer cross sections for NF_3 (10^{-16} cm^2).

Angle (deg)	4 eV	5 eV	7 eV	8 eV	10 eV	15 eV	20 eV	25 eV	30 eV	50 eV	60 eV
0	3.31	2.90	10.67	11.59	9.10	8.07	8.47	9.99	11.87	15.58	17.71
10	15.19	2.85	10.08	10.92	8.57	7.51	7.70	8.76	10.16	12.38	13.47
20	7.59	2.72	8.53	9.13	7.18	6.05	5.77	5.91	6.31	6.15	5.84
30	2.27	2.50	6.52	6.81	5.35	4.22	3.59	3.09	2.85	2.02	1.65
40	0.91	2.21	4.58	4.59	3.58	2.57	1.92	1.40	1.13	0.86	0.87
50	0.82	1.86	3.08	2.93	2.25	1.47	1.03	0.82	0.77	0.79	0.78
60	0.61	1.50	2.14	1.94	1.46	0.95	0.76	0.77	0.83	0.67	0.55
70	0.39	1.18	1.64	1.47	1.11	0.82	0.77	0.79	0.77	0.44	0.35
80	0.26	0.93	1.42	1.28	0.97	0.83	0.78	0.69	0.56	0.26	0.24
90	0.19	0.77	1.30	1.17	0.89	0.78	0.69	0.52	0.35	0.17	0.18
100	0.16	0.68	1.20	1.05	0.79	0.68	0.56	0.40	0.25	0.15	0.16
110	0.22	0.64	1.09	0.90	0.68	0.57	0.49	0.40	0.30	0.27	0.26
120	0.42	0.64	1.00	0.77	0.58	0.53	0.54	0.54	0.51	0.54	0.48
130	0.65	0.68	0.99	0.69	0.55	0.59	0.70	0.81	0.85	0.83	0.71
140	0.89	0.74	1.13	0.71	0.58	0.71	0.93	1.17	1.29	1.09	0.96
150	1.24	0.82	1.43	0.83	0.66	0.88	1.20	1.61	1.81	1.38	1.36
160	1.74	0.90	1.82	1.02	0.77	1.04	1.47	2.06	2.33	1.71	1.86
170	2.14	0.97	2.16	1.20	0.86	1.17	1.67	2.40	2.72	1.94	2.20
180	2.30	1.00	2.29	1.27	0.90	1.21	1.75	2.54	2.87	2.01	2.30
ICS	15.88	14.66	28.26	26.10	20.19	16.62	15.49	15.30	15.18	13.09	12.62
MTCS	10.76	10.76	18.08	14.31	10.98	10.18	10.64	11.49	11.50	9.04	8.65

show the DCSs at 15, 20, 25, 30, 50 and 60 eV, which are energies above the resonance region. At these energies we found again good agreement between our results and experiment. In figure 6 we present our calculated MTCS obtained under the SE approximation along with the results of Boesten *et al* and the complex Kohn results of Rescigno, both under the SE and static-exchange-plus-polarization (SEP) approximations. Our MTCS shows the same shape as the SE results of Rescigno, but our resonance position is shifted to lower energy in comparison with his (by $\sim$1 eV). The SEP results of Rescigno show that the resonance peak moves to lower energy, as expected. At energies above the resonance our results lie above the experimental points. Our results are also presented in table 2.

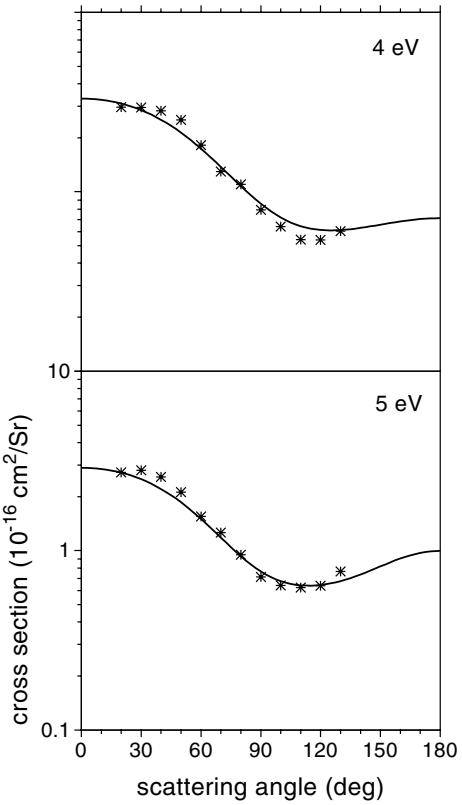

Figure 2. DCSs for NF_3 at 4 and 5 eV.

5. Discussion

Since we have performed a SE e^-–NF_3 collision calculation, the position of our shape resonance is shifted to higher energy. It is well known that polarization effects are very important in giving the right position of a resonance. However, since the existence of this shape resonance has been confirmed by the calculations of Rescigno which take polarization into account, and also by the experimental results of Boesten *et al*, we can extract some additional information about this shape resonance from our calculations.

Although Rescigno showed the existence of a structure in the NF_3 MTCS, he has not assigned it to any representation of the C_{3v} group. Boesten *et al* assigned the resonance to the E representation of the C_{3v} group. Our results have shown that the peak seen in the present calculated ICS is in fact a superposition of two independent shape resonances belonging to the A_1 and E representations of this group.

The formation of a shape resonance can be viewed as the trapping of the incoming electron into an unoccupied (virtual) molecular orbital [19]. Boesten *et al* have reported that for NF_3 this orbital belongs to the E representation of the C_{3v} group. As discussed above, the symmetry decomposition of our ICS shows two independent shape resonances in the E and the A_1 representations of this group. In order to explore the nature of the resonant orbitals, we have carried out a minimal STO-6G basis set calculation using the package GAMESS [20]. The results of this calculation show that the lowest unoccupied E orbital has σ^*(N–F) character,

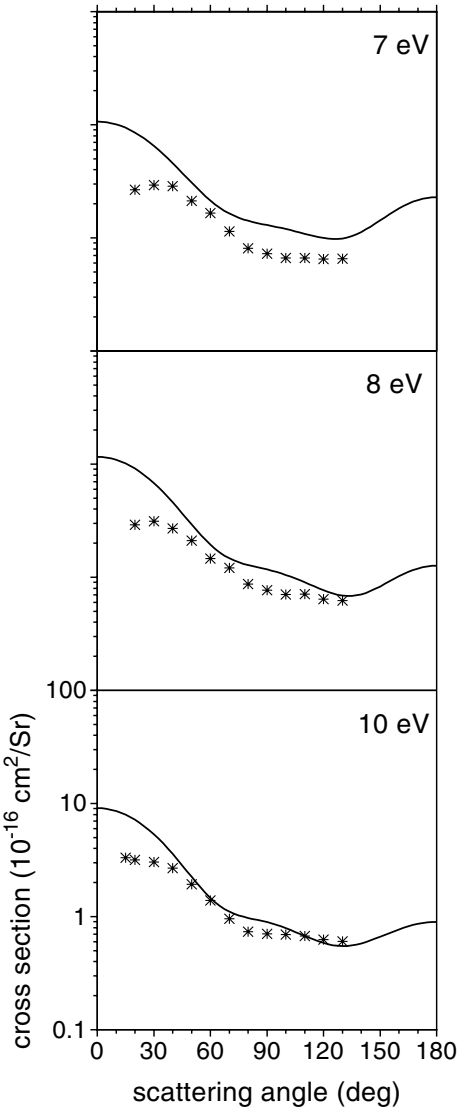

Figure 3. DCSs for NF_3 at 7, 8, and 10 eV.

dissociating the molecule along the N–F bond; we have no definite answer as regards the lowest A_1 unoccupied orbital, although it also seems to be an antibonding orbital.

It has been reported that NF_3 dissociates through electron attachment, where the dominant channel is given by

$$NF_3 + e^- \longrightarrow NF_2 + F^-.$$

In a low-energy electron–molecule collision process the dissociative electron attachment occurs through a shape resonance. It has been pointed out by Rescigno that the NF_3 shape resonance could be responsible for the dissociative attachment of this molecule. Our results give support to the conclusions reported by Rescigno and also support the assertion that the dissociative attachment produces the F^- ion.

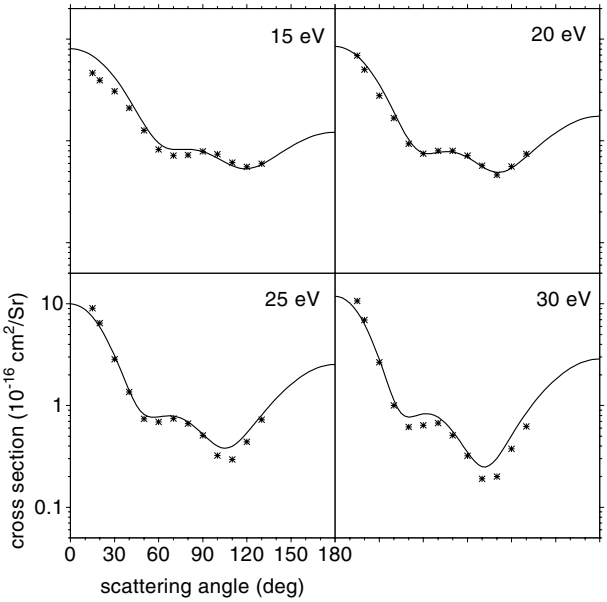

Figure 4. DCSs for NF_3 at 15, 20, 25, and 30 eV.

It should be noted that the two components of the E representation, shown in figure 1, agree very well with each other, but they are not identical. The very small discrepancies seen between the curves result from the numerical quadrature used in the representation of the Green function. The use of larger quadratures will improve the agreement between these cross sections but will not affect the final results. We have found in our E cross section two small spurious structures, one for E_x and the other for E_y, around 4 and 5 eV respectively. We have removed from our configuration space two configurations, one for each component of the E representation, whose energies were just at the spurious structures. This procedure has not affected the final results, giving cross sections free of these structures.

Although our DCSs agree well with the experiment for energies away from the resonance region, as seen in figures 1–3, our ICS and MTCS do not show good agreement with the experimental results. The experimental ICS and MTCS have been obtained from the integration of the measured DCSs after their extrapolation to 0° and 180°. NF_3 has a very small dipole moment and therefore the effect of the dipole interaction is very small and has little effect on the DCSs (the effect is mainly at very low scattering angles and at lower energies [18]). In this case, one can extrapolate the measured DCS to a finite value at 0°, and then make a comparison with the calculated DCS, without worrying about the rise of the DCS near the forward direction [6, 21]. In order to try to explain the discrepancy between theory and experiment seen in the ICS and MTCS we have done the following. We have chosen the DCS at 20 eV, the energy where we have found better agreement between theory and experiment and where we expected the ICS and MTCS to also show good agreement. We then integrated the DCS in two different ways. In order to obtain the ICS we integrated the DCS as follows

$$\mathrm{ICS} = 2\pi \int_0^\pi \mathrm{d}\theta \sin\theta \,\mathrm{DCS}(\theta)$$

and to obtain the MTCS we integrated the DCS as follows:

$$\mathrm{MTCS} = 2\pi \int_0^\pi \mathrm{d}\theta \sin\theta \,(1 - \cos\theta)\,\mathrm{DCS}(\theta).$$

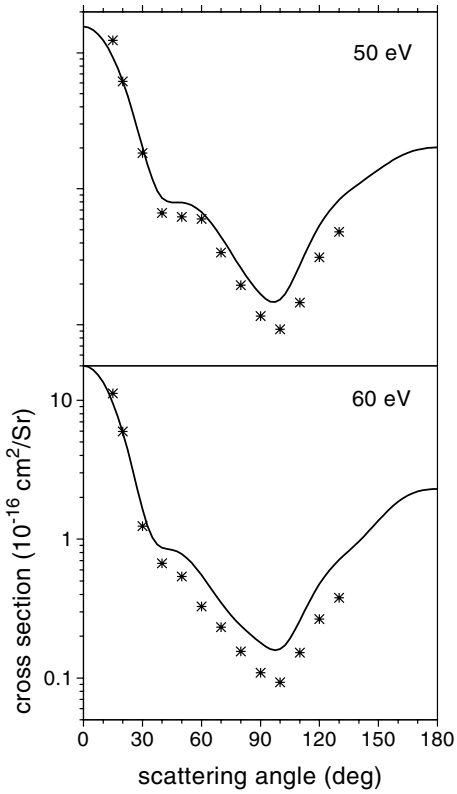

Figure 5. DCSs for NF_3 at 50 and 60 eV.

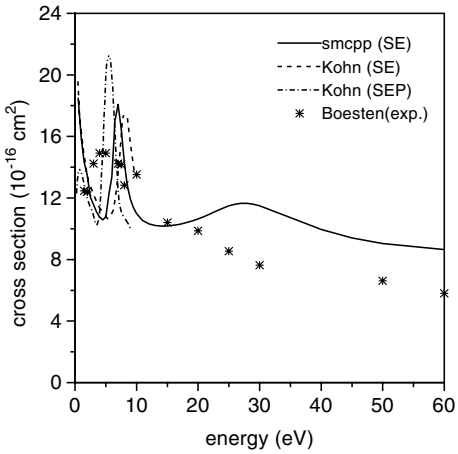

Figure 6. The MTCS for NF_3.

The integration of our calculated DCS gives 15.33 and 10.58×10^{-16} cm^2 for the ICS and MTCS respectively. These values lie above the experimental values of 14.48 and 9.87×10^{-16} cm^2. We then 'extrapolated' the experimental DCS to 0° and to 180° using our calculated DCS at 0°

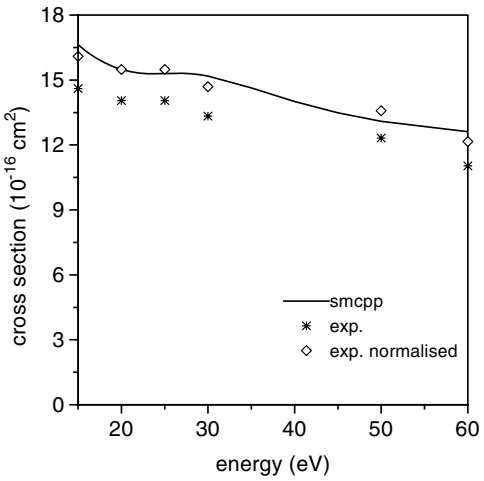

Figure 7. The ICS for NF_3. The experimental points are normalized to ours at 20 eV.

and 10°, in the small-scattering-angles region, and from 140° to 180°, with a step of 10°, in the higher-scattering-angles region. With this procedure, the integration of this 'mixed' DCS gives 14.45 and 10.56 $\times$ 10^{-16} cm^2 for the ICS and MTCS respectively. Although the ICS remains almost unchanged, the MTCS is in good agreement with our value of 10.58 $\times$ 10^{-16} cm^2 reported above. If we now replace the experimental DCS values at 20° and 30° (where theory and experiment show a small discrepancy) by ours in this 'extrapolation', the integration of the resulting 'mixed' DCS gives 15.18 and 10.64 $\times$ 10^{-16} cm^2 for the ICS and MTCS respectively, which are in better agreement with the values reported above of 15.33 and 10.58 $\times$ 10^{-16} cm^2 respectively. We then believe that the discrepancy between theory and experiment seen in the ICS and MTCS plots may be attributed to the small differences between the calculated and measured DCSs and also to the extrapolation of the experimental points to 0° and 180°. We have normalized the experimental ICS to ours at 20 eV, where we have found better agreement between the two DCSs. The result of this procedure is presented in figure 7, which shows good agreement between theory and the experiment after this normalization procedure.

6. Summary

We have presented elastic integral, differential and momentum-transfer cross sections for e^-–NF_3 collision. Our ICS presents two independent shape resonances around 7 eV. A resonant behaviour was also seen in the complex Kohn calculations of Rescigno and in the experiments of Boesten *et al*. Our results confirm the resonance assignment by Boesten *et al* to the E representation of the C_{3v} group and report the existence of another resonance in the A_1 representation of this group. It has been found that NF_3 dissociates through electron attachment and that F^- is the most important channel. We found that the resonant E orbital appears to be of σ^*(N–F) character, leading to the dissociation of the molecule along this bond, while the A_1 orbital seems to be an antibonding orbital.

Acknowledgments

MHFB acknowledges support from the Brazilian agency Conselho Nacional de Desenvolvimento Científico e Tecnológico (CNPq) and from the Paraná state agency Fundação Araucária.

The authors acknowledge Professor Marco A P Lima and Professor Milton M Fujimoto for many helpful discussions and also Professor Carlos M de Carvalho for computational support at Departamento de Física da Universidade Federal do Paraná. Our calculations were performed at the CENAPAD-SP and at DF-UFPR.

References

[1] See, for example, Pruette L, Karecki S, Chatterjee R, Reif R, Sparks T and Vartanian V 2000 *J. Vac. Sci. Technol.* A **18** 2749
LaRoche J R, Ren F, Lothian R, Hong J, Pearton S J, Lambers E, Hsu C H, Wu C S and Hoppe M 2000 *J. Vac. Sci. Technol.* B **18** 283
Kastenmeier B E E, Oehrlein G S, Langan J G and Entley W R 2000 *J. Vac. Sci. Technol.* A **18** 2102
Jenichen A 1995 *Surf. Sci.* **331–3** 1503
Bruno G, Capezzuto P, Cicala G and Manodoro P 1994 *J. Vac. Sci. Technol.* A **12** 690
[2] Little T W and Ohuchi F S 2000 *Surf. Sci.* **445** 235
Endou A, Little T W, Yamada A, Teraishi K, Kubo M, Ammal S S C, Miyamoto A, Kitajima M and Ohuchi F S 2000 *Surf. Sci.* **445** 243
[3] Veilleux J M, El-Genk M S, Chamberlin E P, Munson C and FitzPatrick J 2000 *J. Nucl. Mater.* **277** 315
[4] Winstead C and McKoy V 2000 *Adv. At. Mol. Opt. Phys.* **43** 111
[5] Rescigno T N 1995 *Phys. Rev.* A **52** 329
[6] Boesten L, Tachibana Y, Nakano Y, Shinohara T, Tanaka H and Dillon M A 1996 *J. Phys. B: At. Mol. Opt. Phys.* **29** 5475
[7] Deutsch H, Becker K, Matt S and Märk T D 2000 *Int. J. Mass Spectrom.* **197** 37
[8] Harland P W and Franklin J L 1974 *J. Chem. Phys.* **61** 1621
[9] Nandi D, Rangwala S A, Kumar S V K and Krishnakumar E 2001 *Int. J. Mass Spectrom.* **205** 111
[10] Aschi M and Grandinetti F 2000 *J. Mol. Struct. (Theochem.)* **497** 205
[11] Bettega M H F, Ferreira L G and Lima M A P 1993 *Phys. Rev.* A **47** 1111
[12] Takatsuka K and McKoy V 1981 *Phys. Rev.* A **24** 2473
Takatsuka K and McKoy V 1984 *Phys. Rev.* A **30** 1734
[13] Lima M A P, Brescansin L M, da Silva A J R, Winstead C and McKoy V 1990 *Phys. Rev.* A **41** 327
[14] Bachelet G B, Hamann D R and Schlüter M 1982 *Phys. Rev.* B **26** 4199
[15] Bettega M H F, Natalense A P P, Lima M A P and Ferreira L G 1996 *Int. J. Quantum Chem.* **60** 821
[16] *CRC Handbook of Chemistry and Physics* 1998 79th edn, ed D R Lide (Boca Raton, FL: Chemical Rubber Company)
[17] Winstead C and McKoy V 1998 *Phys. Rev.* A **57** 3589
[18] Varella M T do N, Bettega M H F, da Silva A J R and Lima M A P 1999 *J. Chem. Phys.* **110** 2452
[19] Winstead C and McKoy V 2001 *J. Chem. Phys.* **114** 7407
[20] Schmidt M W *et al* 1993 *J. Comput. Chem.* **14** 1347
[21] Okamoto Y, Onda K and Itikawa Y 1993 *J. Phys. B: At. Mol. Opt. Phys.* **26** 745